Simple capillary-based extrinsic Fabry–Perot interferometer for strain sensing

Xiaobei Zhang (张小贝)*, Haiyang Shao (邵海洋), Haiyang Pan (潘海阳), Yong Yang (杨 勇), Huawen Bai (白化文), Fufei Pang (庞拂飞), and Tingyun Wang (王廷云)

Laboratory of Specialty Fiber Optics and Optical Access Networks, School of Communication and Information Engineering, Shanghai University, Shanghai 200072, China

**Corresponding author: xbzhang@shu.edu.cn*

Received January 2, 2017; accepted March 24, 2017; posted online April 7, 2017

A simple capillary-based extrinsic Fabry–Perot structure is presented and fabricated, using the manual welding method with the strain sensing characteristics investigated in detail. Strain sensitivities of 4.2, 2.8, and 2.4 pm/με are obtained experimentally with the interferometer length around 50 μm and the inner diameter of 75, 50, and 25 μm, respectively. The underlying physics of the strain sensitivity of this device is negatively correlated with the interferometer length and positively correlated with the capillary inner diameter, which provides two simple parameters to tailor the strain sensitivity.

OCIS codes: 060.2370, 050.2230.
doi: 10.3788/COL201715.070601.

All-fiber sensors have been extensively studied due to their competitive superiorities of electromagnetic immunity, light weight, small size, resistance to harsh environments, etc. As one kind of fiber sensing device, fiber-based strain sensors have also been extensively studied. To fabricate optical fiber strain sensor structures, many types of optical structures have been developed successfully with optical fibers, such as the optical fiber Bragg grating[1,2], the long period fiber gratings[3,4], the fiber Mach–Zehnder interferometer[5–7], and the S-tapered fiber sensor structure[8]. The fiber sensor devices mentioned above can be used for strain sensing. However, there are some disadvantages, such as the difficulty to process, low sensitivity, and high cost. Fabry–Perot interferometers (FPIs) have been widely used in a variety of sensing areas in recent years, for example, the pressure[9,10], the refractive index (RI)[11,12], and the strain[13–15] measurements, due to the advantages of the all-fiber sensors mentioned above. As a special hollow core fiber, the capillary is very suitable for fabricating FPIs based on the in-fiber air cavity because of its own hollow core. The capillary provides a simple way to fabricate FPIs for all-fiber devices with various functions. Some Fabry–Perot (FP) cavities have been successfully demonstrated to measure the pressure[16] and the thermal coefficient of the liquids[17].

In this Letter, we propose a capillary-based FP structure and study the characteristics of the device in detail under kinds of capillaries with different interferometer lengths and inner diameters (IDs). The fabrication process is first presented, and then various capillary-based extrinsic FP devices are demonstrated with the strain sensing characteristics investigated. The strain sensitivities are also studied under various interferometer lengths and capillary IDs, which show good potential for compact and low-cost strain sensors.

The proposed capillary-based fiber sensor structure was formed by two glass/air reflection mirrors, and a short segment of capillary used as the interferometer cavity. The smooth welding end face can avoid large insertion loss, and it is also a guarantee for the high contrast of the reflection spectrum. Therefore, in the welding process, we set the discharge current as weak and move the capillary away from the electrode to ensure smoothness of the welding surface. As shown in Fig. 1(a), the detailed processing steps follow.

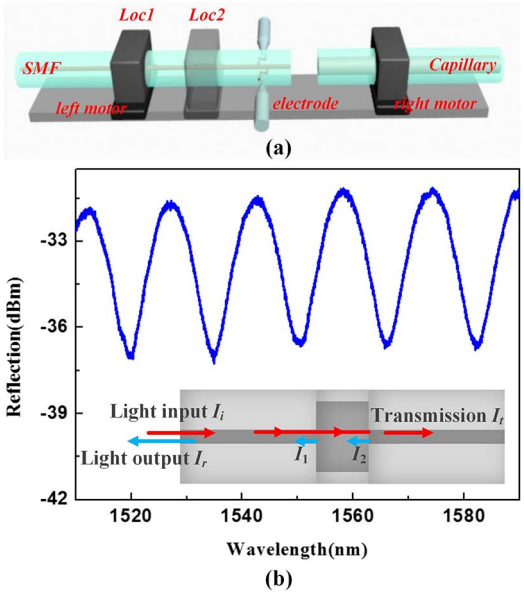

Fig. 1. (a) Illustration for fabricating the device, and (b) the reflection spectrum of the capillary-based FPI. Inset shows the propagation paths of the input and output light in the sensor device.

Table 1. Main Fusion Splicing Parameters in the Experiments

Splicer Parameters	Cleaning Arc Time	Gap	Promoting Distance	Arc Power	Pre-fuse Time	Fuse Time
Data	20 ms	15 μm	20 μm	10 bits	100 ms	500 ms

We adopted three types of quartz capillaries from Polymicro Techologies to implement the proposed FPI sensor. The ID r of the capillaries is about 75 μm (TSP075150), 50 μm (TSP050150), and 25 μm (TSP025150) with the outer diameter 150 μm. When the polymer coating of the capillary is removed by the burning method, the outer diameter R becomes 125 μm. This is comparable to the outer diameter of the single mode fiber (SMF), which makes the fusion of the capillary and the fiber together simple and convenient. We use a segment of capillary and a segment of SMF28 fixed on the stepper motors of a commercial fusion splicer (FITEL-S178). According to demand, we modify the preset splice parameters of the fusion splicer. The cleaning arc time, gap, promoting distance, arc power, pre-fuse time, and fuse time are key parameters in the experiment and critical for fabricating the device, which is summarized and listed as shown in Table 1. In fact, a relatively low level of arc power and shorter discharge time are very important to avoid the collapse of the air hole of the capillary. The tip of capillary keeps a distance from the discharge electrode to avoid the collapse. As shown in Fig. 1(a), the left motor moves forward from position $Loc1$ to position $Loc2$, the promoting distance is 20 μm. After the welding process, only a short segment of capillary is retained by using a normal fiber cleaver under a microscopic imaging system. Finally, the FP cavity can be formed by splicing the cleaved capillary segment with another SMF tip, according to the above method, to form the other mirror. As shown in Fig. 1(b), the standard and typical FP cavity interference spectrum can be obtained, which is formed by the reflecting beams from the two glass/air interfaces marked as I_1 and I_2, respectively, with I_i as the incident light. The output light intensity of the interferometer[15] marked as I_r can be expressed as the well-known two beam interference equation $I_r = I_1 + I_2 + 2\sqrt{I_1 I_2}\cos(4\pi nL/\lambda)$. Here, n is the RI of the gas in the FP cavity, L is the length of the FP cavity, and λ is the wavelength in free space.

The capillary (TSP050150) is adopted first to demonstrate the simple capillary-based extrinsic FPI. The length of the capillary is very important for the FPI. We control the length of the capillary with a normal fiber cleaver and a microscopic imaging system. A capillary with one end welded to an SMF is fixed on the cleaver. Then, the cleaver is placed on the stage under the microscopic imaging system. Through the microscopic imaging system, it is possible to roughly estimate the distance from the blade to the fusion point. Figure 2(a) shows the reflection spectra with the interferometer length L as 55, 85, and 166 μm,

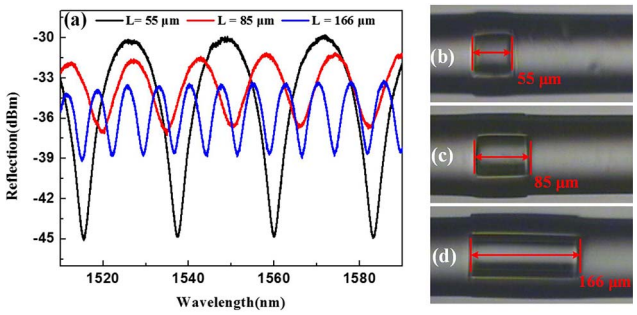

Fig. 2. (a) Reflection spectra of the fabricated FPI devices with different interferometer lengths and the capillary ID of 50 μm. (b)-(d) Microscopic images of fabricated FPI devices.

respectively. Free spectral range (FSR) can be calculated according to FSR $= \lambda^2/(2nL)$. The calculated FSR results are 22, 14, and 7 nm, respectively, which show a good agreement with the experimental results, as shown in Fig. 2(a). Furthermore, both the maximum reflection intensity and the contrast are decreasing as the length of the FP cavity is increasing, which is mainly because the insertion loss increases. The total insertion loss is defined as the difference between the transmission I_t and the input I_i, which can usually be calculated as the decibel (dB) form $10\lg(I_t/I_i)$. A traditional testing configuration with a broadband light source, the device, and the optical spectrum analyzer can be used to get the total insertion loss for the device with an ID of 50 μm. The insertion losses are measured around −3.5, −4.0, and −6.7 dB for the cavity lengths as 55, 85, and 166 μm, respectively, which is shown in Fig. 3. Generally, the total insertion loss is related to the loss of the two glass/air interfaces and the cavity.

The optical path difference of the FP cavity can be expressed as $\delta = 2nL$. As the RI of the air inside the capillary

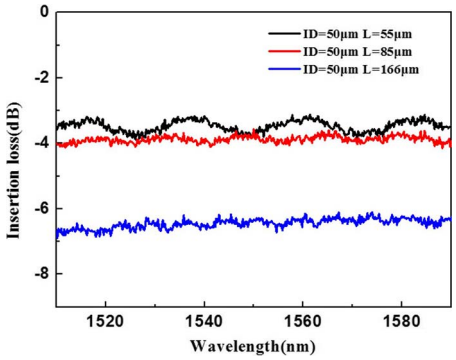

Fig. 3. Measured insertion loss for the devices with an inner capillary diameter of 50 μm.

is near constant, the axial stress will not change its RI. For the capillary, the outer diameter and ID are R and r, respectively. When the force F is applied to the FP sensor, the change of the optical path difference can be expressed as $\Delta\delta = \delta \cdot \varepsilon = \delta \cdot F/[\pi(R^2 - r^2)E]$[4,8]. $\varepsilon = \Delta L/L$ is the axial strain, and E is the Young's modulus of the capillary.

Figure 4 shows the setup for carrying out the strain sensing experiment. The reflection spectra are measured using the optical sensing analyzer Si725 (Micron Optics Inc.) with a resolution of 0.005 nm. The FP sensor is fixed with a fiber clamp and a digital dynamometer (Nidec Shimpo FGJ-1). The spectrum is recorded from 0 to 1000 με with the steps of 100 με. We experimentally studied the relationship between the strain sensing characteristics under different device lengths. For the FP device with the capillary length of 55 μm and ID of 50 μm, the red shift phenomenon appears as the strain increases, as shown in Fig. 5(a). A linear relationship of the wavelength shift is observed as the axial strain applied to the FP sensor. Furthermore, we carried out the strain sensing experiments for lengths of 85 and 166 μm. Wavelength shifts show the same trend, which are also nearly linear. Moreover, the strain sensing sensitivity is larger under the shorter cavity length, as shown in Fig. 5(b). Strain sensing sensitivities of 2.8, 2.3, and 1.9 pm/με are obtained as the cavity lengths are 55, 85, and 166 μm, respectively. This suggests that a smaller interferometer length will enhance the strain sensitivity.

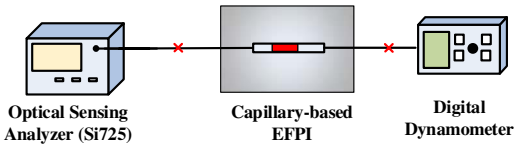

Fig. 4. Illustration of the strain sensing experimental setup. EFPI, extrinsic FPI.

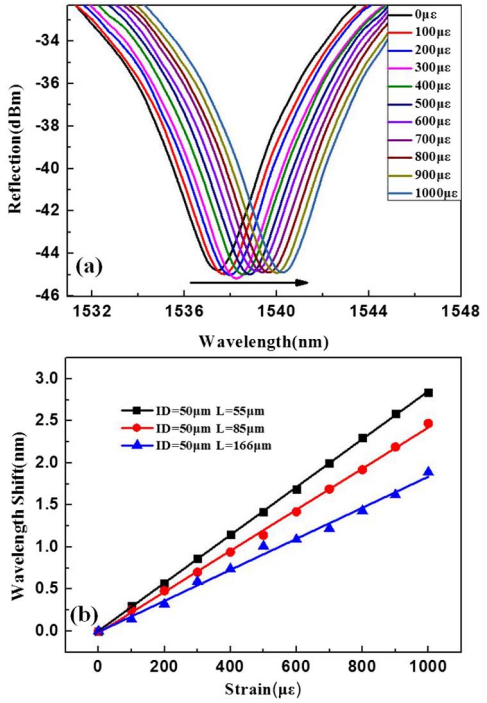

Fig. 5. (a) Spectral shift as the strain increases from 0 to 1000 με for the device with ID = 50 μm and $L = 55$ μm, and (b) the response of the strain with different FP cavity lengths.

Moreover, the strain sensing characteristics of the FP devices based on the capillaries with the IDs of 75 and 25 μm, also exhibit the same trend, as shown in Fig. 5. The strain sensing sensitivities of 4.2, 2.9, and 2.3 pm/με are obtained for the cavity lengths of 53, 102, and 186 μm, respectively, when the capillary ID is 75 μm. We also obtain the strain sensing sensitivities of 2.4, 1.8, and 1.6 pm/με when the cavity lengths are 56, 103, and 163 μm, respectively, when the capillary ID is 25 μm. The strain sensitivities as functions of the interferometer length and the capillary ID are summarized, as shown in Fig. 6. The strain sensitivity of this device is negatively correlated with the interferometer length and positively correlated with the capillary ID. In this way, we can adopt two simple parameters, such as the interferometer length and ID, to tailor its strain sensitivity efficiently. The repeatability and stability of the fabricated device also show a good performance due to the manual welding technology without any additional processing steps, such as tapering or etching.

In conclusion, a capillary-based FPI is demonstrated in this Letter by manual welding technology. We investigate the strain sensing characteristics of the sensor device under different capillary interferometer lengths and IDs. Through this simple optical device, strain sensitivities of 4.2, 2.8, and 2.4 pm/με can be obtained experimentally with the interferometer length around 50 μm and the IDs of 75, 50, and 25 μm, respectively. The strain sensing sensitivity is found to be negatively correlated with the length of the device and positively correlated with the capillary ID. The effective way to enhance the strain sensing sensitivity is fabricating this simple capillary-based extrinsic FPI with a shorter cavity length under the larger ID.

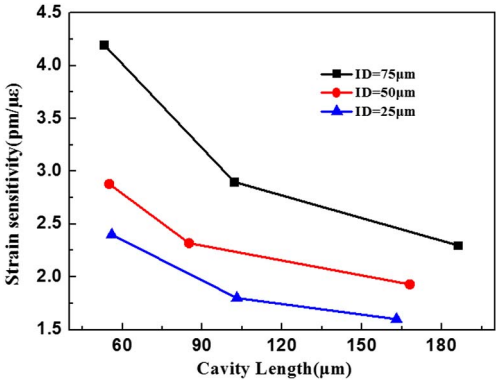

Fig. 6. Strain sensitivity of the sensor devices with different IDs and interferometer lengths.

This work was supported by the National Natural Science Foundation of China (Nos. 61675126, 61377081, and 61007035) and the Chen Guang Project by the Shanghai Municipal Education Commission and Shanghai Education Development Foundation (No. 12CG48).

References

1. C. Chen, A. Laronche, G. Bouwmans, L. Bigot, Y. Quiquempois, and J. Albert, Opt. Express **16**, 9645 (2008).
2. Y. J. Rao, X. K. Zeng, Y. Zhu, Y. P. Wang, T. Zhu, Z. L. Ran, L. Zhang, and B. Ian, Chin. Phys. Lett. **18**, 643 (2001).
3. Q. Huang, Y. Yu, S. Ruan, and X. Li, IEEE Photon. Technol. Lett. **27**, 1216 (2015).
4. H. Zeng, T. Geng, W. Yang, and M. An, IEEE Photon. Technol. Lett. **28**, 1 (2015).
5. C. R. Liao, D. N. Wang, and Y. Wang, Opt. Lett. **38**, 757 (2013).
6. Y. S. Zhang, X. G. Qiao, M. Shao, and Q. M. Liu, Chin. Phys. Lett. **32**, 84 (2015).
7. J. C. Shin, W. G. Kwak, and Y. G. Han, J. Lightwave Technol. **34**, 4579 (2016).
8. R. Yang, Y. S. Yu, C. Chen, Y. Xue, X. L. Zhang, J. C. Guo, C. Wang, F. Zhu, B. L. Zhang, and Q. D. Chen, J. Lightwave Technol. **30**, 3126 (2012).
9. B. Sun, Y. Wang, J. Qu, C. Liao, G. Yin, J. He, J. Zhou, J. Tang, S. Liu, and Z. Li, Optics Express **23**, 1906 (2015).
10. C. Wu, H. Y. Fu, K. K. Qureshi, B. O. Guan, and H. Y. Tam, Opt. Lett. **36**, 412 (2011).
11. P. Liu, L. Jiang, S. Wang, Z. Cao, and P. Wang, Chin. Opt. Lett. **14**, 020602 (2016).
12. X. Zhang, J. Xiong, F. Gu, J. Li, W. Wang, F. Pang, and T. Wang, Chin. Opt. Lett. **13**, 18 (2015).
13. S. Liu, Y. Wang, C. Liao, G. Wang, Z. Li, Q. Wang, J. Zhou, K. Yang, X. Zhong, and J. Zhao, Opt. Lett. **39**, 2121 (2014).
14. D. W. Duan, Y. J. Rao, L. C. Xu, T. Zhu, M. Deng, D. Wu, and J. Yao, Opt. Commun. **284**, 5311 (2011).
15. X. Zhang, W. Peng, and Y. Zhang, Opt. Lett. **40**, 5658 (2015).
16. B. Xu, C. Wang, D. N. Wang, Y. Liu, and Y. Li, Opt. Express **23**, 23484 (2015).
17. C. L. Lee, H. Y. Ho, J. H. Gu, T. Y. Yeh, and C. H. Tseng, Opt. Lett. **40**, 459 (2015).